Original Paper

Special issue : Frontiers of Vibrational Spectroscopy in Analytical Chemistry.

Effect of Casting Solvent on Interfacial Molecular Structure and Proton Transport Characteristics of Sulfonated Polyimide Thin Films

Yuki NAGAO,*† Karthik KRISHNAN,* Ryosuke GOTO,** Mitsuo HARA,** and Shusaku NAGANO***

* *School of Materials Science, Japan Advanced Institute of Science and Technology, 1-1 Asahidai, Nomi, Ishikawa 923-1292, Japan*

** *Department of Molecular Design & Engineering, Graduate School of Engineering, Nagoya University, Furo-cho, Chikusa, Nagoya 464-8603, Japan*

*** *Nagoya University Venture Business Laboratory, Nagoya University, Furo-cho, Chikusa, Nagoya 464-8603, Japan*

† To whom correspondence should be addressed.

E-mail: ynagao@jaist.ac.jp

K. K. present address: International Center for Materials Nanoarchitectonics (MANA), National Institute for Materials Science, 1-1 Namiki, Tsukuba, Ibaraki 305-0044, Japan.

Abstract

Two sulfonated polyimide (SPI) thin films were prepared with water and THF/water mixed solvents, respectively. The SPI thin film prepared with THF/water showed more than 5 times higher proton conductivity than that prepared with water mixed solvent at low relative humidity (RH) and 298K. In this study, polarized optical microscopy (POM), grazing incidence small angle X-ray scattering (GISAXS), and p-polarized multiple angle incidence resolution spectrometry (pMAIRS) were carried out to investigate liquid crystalline (LC) optical ordered structure, organized structure, and molecular orientation. The molecular ordered parts using LC properties in the SPI thin films exhibited an almost identical structure under the low RH condition. On the other hand, the molecular orientation of the imide C=O groups in the non-ordered parts, which could not be detected by POM and GISAXS, showed different angles. The proton conductivity under low RH conditions is affected by the degree of the molecular orientation in the non-ordered parts of the SPI thin films.

Keywords MAIRS, proton conductivity, surface morphology, molecular ordering, molecular orientation

(Received August 18, 2016; Accepted September 23, 2016; Published January 10, 2017)

Introduction

Advanced polymer electrolyte membranes (PEMs) have been developed in recent years for their wide range of applications, particularly in the area of fuel cell applications.[1-4] Performance improvement requires structural controls over molecular orientations and organized structure of ionomers in PEMs. Recently, structural confinement effects of polymer in nanostructured thin films have been intensively investigated because morphology and chain dynamics of polymer thin films are significantly affected by surfaces and substrate interface. [5-13] The confinements in thin films induce preferred chain packings and molecular orientations along the in-plane or out-of-plane direction from a substrate plane by self-assembly, which exhibits the highly organized ion-conducting channels that possibly lead to the change of transport characteristics.[14-19] Therefore, the organized structure has attracted considerable interest for high proton conduction in thin films.

Sulfonated polyimides (SPIs) are one of the promising candidates for essential polymer electrolytes for fuel cells due to their thermal and chemical stabilities.[14-16,20-35] In thin films, aromatic polyimides (PIs) possessing a rigid and planar backbone exhibit a highly ordered lamella structure oriented parallel to the substrate plane with in-plane orientated backbones.[36] Notably, the molecular structure and *ch*-packing of imide and phenyl groups in PIs significantly vary depending on the aggregation structures, such as crystalline, liquid crystalline-like and amorphous. In our previous studies, we have found the lyotropic liquid crystalline (LC) lamellar behavior in the SPI thin film and existence of high relative humidity (RH) induces the expansion of the LC structure to the out-of-plane direction. Owing to the large scaled LC ordering and interchain *ch*-packing of SPI thin films, the proton transport characteristic is much improved in the high humidified condition.[14] On the other hand, the SPI thin film has a less molecular ordered structure under low RH conditions. In the low RH atmosphere, the proton

conduction path has not been discussed yet. The SPI thin film has well-organized parts and non-ordered parts, which could not be detected by polarized optical microscopy (POM) and X-ray scattering in low RH conditions. Therefore, the characterization techniques for both parts of the SPI thin film are essential to investigate the factors of the proton conductivity.

In one study of this issue, we focused on the effect of a spin casting solvent. It is noteworthy that the degrees of molecular ordering and interchain polymer interaction are also dependent on the deposition solvents. Solvents applied for film preparation can normally affect the polymer microstructure.[37-42] For instance, Chang *et al*. reported that the high boiling solvents can lead to extensive crystallization in thin films and poorer solvents exhibited poorly ordered chain aggregates at film interaces.[39] Furthermore, the polymer orientation and interchain interaction of polymer chains are strongly dependent on the solvent evaporation speed during film preparation; this is because the volume shrinkage of the polymer films causes a preferential chain alignment.

During our consideration of the spin casting solvents, we found that the proton conductivity strongly depends on the deposition solvents. Therefore, we aim to reveal a fundamental understanding of how the casting solvent affects the polymer structure in SPI thin films. Because tetrahydrofurane (THF) enhances solubility for the SPI, two solvent systems such as polar protic (milli-Q water, denoted as “without THF”) and mixtures of polar protic and an aprotic (THF, denoted as “with THF”) solvents for casting the SPI films on substrates were chosen. To investigate the difference of the proton conductivity in the two SPI thin films prepared with THF and without THF, both well-organized parts and non-ordered parts were discussed from the viewpoint of the LC ordered structure, organized structure, and molecular orientation. Changes in the interfacial molecular structure by different solvents can be responsible for the obvious changes in the proton transport characteristics of SPI thin films.

Experimental

Reagents and chemicals

3,3'-Dihydroxybenzidine, propanesultone, and pyromellitic dianhydride were used as received from TCI, Japan. Acetic anhydride, acetic acid, methanol, acetone, and THF were purchased from Wako Chemicals, Japan. Hydrochloric acid (Nacalai Tesque, Japan), sodium hydroxide (Kishida Chemical, Japan), m-cresol, and triethylamine (TEA) (Kanto Chemicals, Japan) were used as received.

Synthesis of SPI

The high molecular weight SPI with a molecular weight of 1.4×10^6 was prepared. Synthesis of SPI has already been reported elsewhere.[14,16] The SPI was characterized by ^{1}H NMR, FT-IR, and gel permeation chromatography. The FT-IR results showed no residual amic acid group.

Preparation of thin films

The highly oriented SPI thin films were prepared on a quartz substrate or Si(100) wafer using a spin cast method (Active ACT−200) with optimized experimental conditions. Dry SPI powders were dissolved in two different solvent systems (polar protic (milli-Q water) and a mixture of an aprotic/protic (THF/milli-Q water). Pure THF is a poor solvent for the SPI. The desired SPI film thickness was obtained by controlling the polymer to solvent ratio. Prior to film deposition, the substrate was subjected to several cleaning processes, and plasma treatment was performed using a vacuum plasma system (Cute-MP; Femto Science, Korea) to improve surface hydrophilicity. The thicknesses of the thin films were measured using a surface profiler (KLA-Tencor P-15 profiler).

Proton conductivity

The proton conductivity of the SPI thin films was examined through impedance spectroscopy measurements using a frequency response analyzer (SI1260; Solartron Analytical) equipped with a high-frequency dielectric interface (SI1296; Solartron Analytical). The RH and temperature were controlled using a computer-controlled environmental test chamber (SH-221; Espec Corp.). RH and temperature were fixed as 40% and 298 K, respectively. The measurement direction was chosen as parallel to the surface of the thin films and porous gold contacts were used as electrodes. The two-probe method was used and impedance data were collected for frequencies of 1 Hz and 10 MHz, with an applied alternating potential of 50 mV. Thin-film conductivity (σ) was calculated as,

$$\sigma = \frac{d}{Rlt} \tag{1}$$

where d signifies the distance between the gold electrodes, R is the resistance value obtained directly from the impedance measurement, l denotes the contact electrode length, and t represents the thickness of the film.

Polarized optical microscopy (POM)

POM was conducted with crossed polarizers to observe the LC ordered domains and to ascertain their size in the polymer films (BX51-P; Olympus Corp. / DP28 camera; Olympus Corp.) Data were recorded with Cellscan controller software.

Grazing incidence small angle X-ray scattering (GISAXS)

GISAXS measurements were performed using an X-ray diffractometer (FR-E; Rigaku Corp.) with an R-AXIS IV two-dimensional (2D) detector. The sample stage was composed of

the goniometer and a vertical stage (ATS-C316-EM/ALV-300-HM; Chuo Precision Industrial Co. Ltd.) with a humidity-controlled cell. The typical cell holds polyimide film (Kapton) windows and the humidity-controlled cell. Nitrogen carrier gas was used as received. Cu Kα radiation (λ = 0.1542 nm) with a beam size of approximately 300 μm × 300 μm was used. The camera length was 300 mm. The incidence angle was chosen in the range from 0.20° to 0.22°. For 1-D out-of-plane and in-plane patterns, the integrated regions were taken between -0.5° to 0.5° as α from the center (0°) and the width of 1° as 2θ, respectively. The RH was controlled at 40%.

p-polarized multiple angle incidence resolution spectrometry (pMAIRS)

The pMAIRS technique was used to investigate the polymer orientations of the nanostructured SPI thin films on Si wafers in both the in-plane and out-of-plane directions.[43,44] The surface of the original Si wafer was natively oxidized before the measurement. The pMAIRS measurements were collected with a Fourier-transform infrared (FTIR) spectrometer (Nicolet 6700; Thermo−Fisher Scientific) equipped with a mercury cadmium telluride (MCT) detector. Single-beam spectra were collected from 38° to 8° in 6° steps between the angle of incidence. Thicknesses of the SPI thin films used in this measurement were approximately 500 nm thick.

Results and Discussion

The conductivity difference between SPI thin films prepared using two different solvent systems has been investigated at low RH. The proton conductivity was found to be 4.1×10^{-4} S cm^{-1} and 7.5×10^{-5} S cm^{-1} at RH = 40%, respectively, in the SPI thin films prepared with THF and without THF solvent. The proton conductivity of the SPI thin film prepared with THF was

much higher than that prepared without THF. This result suggests that the solvent system for the SPI thin film preparation strongly affects proton conductivity in a low humidity atmosphere.

Our recent work demonstrated that the SPI thin films exhibit the molecular ordering using the LC property.[14,16] To check the difference of the molecular ordering, we observed internal morphology of the films by POM. Figure 1 shows the POM images of SPI thin films prepared with two different solvent systems. According to the birefringence images, the LC domain sizes of both films reached more than several micrometers. Both SPI thin films show similar lyotropic LC optical domain sizes and morphologies, which suggests that the LC regions within the domains are essentially unchanged in both films. We conclude that there is no apparent effect for the change of the LC domain size between two spin casting solvents. These LC optical domains reveal the LC ordering structure in the SPI thin films.

The SPI thin film exhibits an LC ordered structure and the degree of the molecular ordering strongly depends on the RH.[14] To clarify the difference between the two SPI thin films prepared with the two spin casting solvents, GISAXS measurements were carried out at RH = 40%. Figure 2 shows GISAXS profiles of the two SPI thin films prepared with THF and without THF. The 2D GISAXS profiles as shown in Figs. 2(a) and 2(b) reveal no characteristic difference. Figure 2(c) shows 1D GISAXS profiles. According to the previous report,[16] the broad peak position of α in the out-of-plane direction depends on the lamellar distance. These α values for the two SPI thin films were similar and we could not find any difference in the width or intensity of the broad GISAXS peaks in either. There is no apparent change of the LC ordered structure of the SPI thin films. The internal structure in the ordered LC domains in the SPI thin film can be regarded as almost identical. To investigate the molecular structures and orientations in the SPI thin films by spectroscopy, pMAIRS analysis was carried out.

The IR pMAIRS technique can provide the opportunity to investigate the in-plane (IP) and out-of-plane (OP) molecular vibrations to the substrate surface in SPI thin films (Fig. 3). In SPI thin films, there are four dominant vibrational modes. Two vibrational modes around 1781 and 1724 cm^{-1} correspond to the C=O symmetric and asymmetric stretching vibrations of imide groups, respectively. Two other peaks at 1504 cm^{-1} and 1381 cm^{-1} correspond to the vibrations of phenyl C−C stretching and C−N bond of the imide groups, respectively.[14, 45-47] The peak position and intensity of vibrational modes for both IP and OP components are taken into account for estimating the molecular orientation by the variation of solvent systems. The spectra absorbance between IP and OP spectra were different in the two SPI thin films.

The vibrational mode for the C−N bond of the imide groups at 1381 cm^{-1} is parallel to the rigid main chain direction. In principle, the anisotropy of polymer orientation gives maximum absorbance strength in the vibrational modes, because of the parallel arrangement of electric field vector and orientated polymer chain vibrations.[48] Observation of the relative increase in absorbance strength of IP component compared to OP component is due to the highly oriented polymer chains parallel to the substrate surface. The characteristic difference of the OP spectra between the two SPI thin films can be seen in the C=O asymmetric vibrational mode at 1736 cm^{-1}. Especially, OP absorbance of the SPI thin film prepared with THF (Fig. 3(a)) was stronger than that of the SPI thin film prepared without THF (Fig. 3(b)). According to the designed polymer structure model, the direction of the sum of this C=O asymmetric vibrational mode at 1736 cm^{-1} should be perpendicular to the direction of the rigid main chain. The increase of the OP peak absorbance for C=O asymmetric vibrational modes can be recognized as a more orientation of C=O groups to the surface normal. Therefore, THF solvent induces a relative edge-on orientation of the imide planar groups in the SPI thin film. The pMAIRS

technique can quantitatively determine the degree of the molecular orientation using the C=O asymmetric stretching mode. It is estimated according to the following equation (2),[49]

$$\varphi = \tan^{-1}\sqrt{\frac{2I_{IP}}{I_{OP}}} \tag{2}$$

where I_{IP} and I_{OP} are the IP and OP peak absorbance of the C=O group and φ is the orientation angle from the surface normal. The obtained angles (φ) of the C=O asymmetric stretching modes are 32° and 45°, respectively, in the SPI thin films prepared with THF and without THF. Therefore, the two SPI thin films have different molecular orientations due to two different spin casting solvents. Previous GISAXS results suggest no characteristic difference in the molecular ordered parts of the two films. The present orientational difference of the molecular orientation could be mainly attributed to the non-ordered parts that are impenetrable by POM and X-ray scattering.

Our previous reports revealed that the enhancement of the proton conductivity coincided with the expansion and ordering for the lamella spacing of the LC phase by adsorbed water with the increase of RH in the SPI film.[14,16] The conductivity enhancement and lamella expansion particularly occur from 40% RH. The present condition of 40% RH is regarded as the state containing low adsorbed water. The present results reveal that the proton conductivity of the SPI films greatly depends on the casting solvents in the less adsorbed water condition. The difference of the conductivity is more than 5 times at low RH. The present spectroscopic results strongly suggest that the chain orientation in the non-ordered parts strongly affects the proton conductivity at low RH. The boundaries of the LC domains mostly constitute the non-ordered part. Therefore, we presume that the proton transport at low RH is dominated by the dry boundary. From spectroscopic evidence, a good solvent with THF and water can make polymer

chains tend to adopt the molecular orientation of imide C=O groups to the surface normal in the non-ordered parts. On the other hand, a poorer solvent with the absence of THF can lead to the planar polymer chain orientation with less polymer tilting in the part of imide rings. As consequence, the chain alignment in thin films on a substrate surface can also be controlled by film casting solvents in low RH. In the previous reports,[14-16] the proton conduction path had not been discussed because of the less ordered structure. In this study, the pMAIRS study enables us to discuss the molecular orientation in the non-ordered parts. Thus, we conclude that the difference of the molecular orientations in the non-ordered parts could strongly affect the proton conductivity at low RH conditions for the SPI thin films.

Conclusions

The casting solvent affects the proton conductivity of the SPI thin film. The molecular ordering by the LC property was identical for the two SPI thin films prepared with THF and without THF. On the other hand, the degree of the molecular orientation in the non-ordered parts was found to be different. In the lower RH condition, the proton conductivity was affected by this difference. This result demonstrates the importance of the characterization between molecular ordered and non-ordered parts in the SPI thin films using spectroscopic studies. The pMAIRS study is one of the powerful methods to investigate the molecular orientation in SPI thin films. The combination with the GISAXS technique provides more useful information on the relationship between the physical property and structure in the molecular ordered and non-ordered parts in the polymer thin films.

Acknowledgements

This work was supported in part by the Nanotechnology Platform Program (Molecule and Material Synthesis) of the Ministry of Education, Culture, Sports, Science and Technology

(MEXT), Japan.

References

1. B. Soberats, M. Yoshio, T. Ichikawa, S. Taguchi, H. Ohno, and T. Kato, *J. Am. Chem. Soc.*, **2013**, *135*, 15286.

2. T. Tamura and H. Kawakami, *Nano Lett*., **2010**, *10*, 1324.

3 R. P. Pandey, A. K. Thakur, and V. K. Shahi, *ACS Appl. Mater. Interfaces*, **2014**, *6*, 16993.

4 O. Kim, G. Jo, Y. J. Park, S. Kim, and M. J. Park, *J. Phys. Chem. Lett.*, **2013**, *4*, 2111.

5 X. C. Chen, D. T. Wong, S. Yakovlev, K. M. Beers, K. H. Downing, and N. P. Balsara, *Nano Lett*., **2014**, *14*, 4058.

6 Y. Daiko, K. Katagiri, and A. Matsuda, *Chem. Mater*., **2008**, *20*, 6405.

7 D. K. Paul, A. Fraser, J. Pearce, and K. Karan, *ECS Trans*., **2011**, *41*, 1393.

8 S. K. Dishari and M. A. Hickner, *Macromolecules*, **2013**, *46*, 413.

9. D. Tanaka, T. Mizuno, M. Hara, S. Nagano, I. Saito, K. Yamamoto, and T. Seki, *Langmuir*, **2016**, *32*, 3737.

10. M. A. Modestino, D. K. Paul, S. Dishari, S. A. Petrina, F. I. Allen, M. A. Hickner, K. Karan, R. A. Segalman, and A. Z. Weber, *Macromolecules*, **2013**, *46*, 867.

11. Y. Nagao, *J. Phys. Chem. C*, **2013**, *117*, 3294.

12. Y. Guo, Y. Ono, and Y. Nagao, *Langmuir*, **2015**, *31*, 10137.

13. Y. Ono and Y. Nagao, *Langmuir*, **2016**, *32*, 352.

14. K. Krishnan, H. Iwatsuki, M. Hara, S. Nagano, and Y. Nagao, *J. Mater. Chem. A*, **2014**, *2*, 6895.

15. K. Krishnan, T. Yamada, H. Iwatsuki, M. Hara, S. Nagano, K. Otsubo, O. Sakata, A. Fujiwara, H. Kitagawa, and Y. Nagao, *Electrochemistry*, **2014**, *82*, 865.

16. K. Krishnan, H. Iwatsuki, M. Hara, S. Nagano, and Y. Nagao, *J. Phys. Chem. C*, **2015**, *119*, 21767.

17. J. Matsui, H. Miyata, Y. Hanaoka, and T. Miyashita, *ACS Appl. Mater. Interfaces*, **2011**, *3*, 1394.

18. Y. Nagao, J. Matsui, T. Abe, H. Hiramatsu, H. Yamamoto, T. Miyashita, N. Sata, and H. Yugami, *Langmuir*, **2013**, *29*, 6798.

19. J. A. Dura, V. S. Murthi, M. Hartman, S. K. Satija, and C. F. Majkrzak, *Macromolecules*, **2009**, *42*, 4769.

20. N. Cornet, O. Diat, G. Gebel, F. Jousse, D. Marsacq, R. Mercier, and M. Pineri, *J. New Mater. Electrochem. Syst.*, **2000**, *3*, 33.

21. C. Genies, R. Mercier, B. Sillion, N. Cornet, G. Gebel, and M. Pineri, *Polymer*, **2001**, *42*, 359.

22. S. Besse, P. Capron, O. Diat, G. Gebel, F. Jousse, D. Marsacq, M. Pineri, C. Marestin, and R. Mercier, *J. New Mater. Electrochem. Syst.*, **2002**, *5*, 109.

23. J. Fang, X. Guo, S. Harada, T. Watari, K. Tanaka, H. Kita, and K. Okamoto, *Macromolecules*, **2002**, *35*, 9022.

24. X. Guo, J. Fang, T. Watari, K. Tanaka, H. Kita, and K. Okamoto, *Macromolecules*, **2002**, *35*, 6707.

25. Y. Yin, J. Fang, Y. Cui, K. Tanaka, H. Kita, and K. Okamoto, *Polymer*, **2003**, *44*, 4509.

26. Y. Yin, J. Fang, H. Kita, and K. Okamoto, *Chem. Lett.*, **2003**, *32*, 328.

27. K. Okamoto, *J. Photopolym. Sci. Technol.*, **2003**, *16*, 247.

28. K. Miyatake, N. Asano, and M. Watanabe, *J. Polym, Sci., Part A: Polym. Chem.*, **2003**, *41*, 3901.

29. T. Watari, J. Fang, K. Tanaka, H. Kita, K. Okamoto, and T. Hirano, *J. Membr. Sci.*, **2004**, *230*, 111.

30. Y. Yin, J. Fang, T. Watari, K. Tanaka, H. Kita, and K. Okamoto, *J. Mater. Chem.*, **2004**, *14*, 1062.

31. Y. Yin, Y. Suto, T. Sakabe, S. W. Chen, S. Hayashi, T. Mishima, O. Yamada, K. Tanaka, H. Kita, and K. Okamoto, *Macromolecules*, **2006**, *39*, 1189.

32. X. Ye, H. Bai, and W. S. W. Ho, *J. Membr. Sci.*, **2006**, *279*, 570.

33. N. Asano, M. Aoki, S. Suzuki, K. Miyatake, H. Uchida, and M. Watanabe, *J. Am. Chem. Soc*., **2006**, *128*, 1762.

34. J. Saito, K. Miyatake, and M. Watanabe, *Macromolecules*, **2008**, *41*, 2415.

35. O. Savard, T. J. Peckham, Y. Yang, and S. Holdcroft, *Polymer*, **2008**, *49*, 4949.

36. J. Wakita, S. Jin, T. J. Shin, M. Ree, and S. Ando, *Macromolecules*, **2010**, *43*, 1930.

37. S. Brinkmann, R. Stadler, and E. L. Thomas, *Macromolecules*, **1998**, *31*, 6566.

38. Y. Funaki, K. Kumano, T. Nakao,H. Jinnai, H. Yoshida, K. Kimishima, K. Tsutsumi, Y. Hirokawa, and T. Hashimoto, *Polymer*, **1999**, *40*, 7147.

39. J. F. Chang, B. Sun, D. W. Breiby, M. M. Nielsen, T. I. Sölling, M. Giles, I. McCulloch, and H. Sirringhaus, *Chem. Mater.*, **2004**, *16*, 4772.

40. P. K. H. Ho, L. L. Chua, M. Dipankar, X. Gao, D. Qi, A. T. S. Wee, J. F. Chang, and R. H. Friend, *Adv. Mater.*, **2007**, *19*, 215.

41. G. Kim and M. Libera, *Macromolecules*, **1998**, *31*, 2569.

42. X. T. Hao, T. Hosokai, N. Mitsuo, S. Kera, K. K. Okudaira, K. Mase, and N. Ueno, *J. Phys. Chem. B*, **2007**, *111*, 10365.

43. T. Hasegawa, *J. Phys. Chem. B*, **2002**, *106*, 4112.

44. T. Hasegawa, *Anal. Chem*., **2007**, *79*, 4385.

45. J. Wakita, H. Sekino, K. Sakai, Y. Urano, and S. Ando, *J. Phys. Chem. B*, **2009**, *113*, 15212.

46. T. Miyamae, K. Tsukagoshi, O. Matsuoka, S. Yamamoto, and H. Nozoye, *Langmuir*, **2001**, *17,* 8125.

47. J. Sung, D. Kim, C. N. Whang, M. Oh-e, and H. Yokoyama, *J. Phys. Chem. B*, **2004**, *108*, 10991.

48. T. Hasegawa, *Anal. Bioanal. Chem*., **2007**, *388*, 7.

49. T. Hasegawa, *Anal. Sci.*, **2008**, *24*, 105.

Figure Captions

Fig. 1 Polarized optical micrograph (POM) images of the 400 nm SPI films at 0º and 45º. (a), (b) SPI thin film prepared without THF. (c), (d) SPI thin film prepared with THF.

Fig. 2 GISAXS profiles of the two SPI thin films at RH = 40%. (a) 2D GISAXS profile of the SPI thin film prepared with THF. (b) 2D GISAXS profile of the SPI thin film prepared without THF. (c) 1D GISAXS profiles in the out-of-plane direction of the two SPI thin films prepared with THF and without THF. Dotted line and solid line are SPI thin films prepared with THF and without THF, respectively.

Fig. 3 pMAIR spectra for the two SPI thin films. (a) SPI thin film prepared without THF. (b) SPI thin film prepared with THF. Solid line and dotted line are OP and 2×IP spectra, respectively.

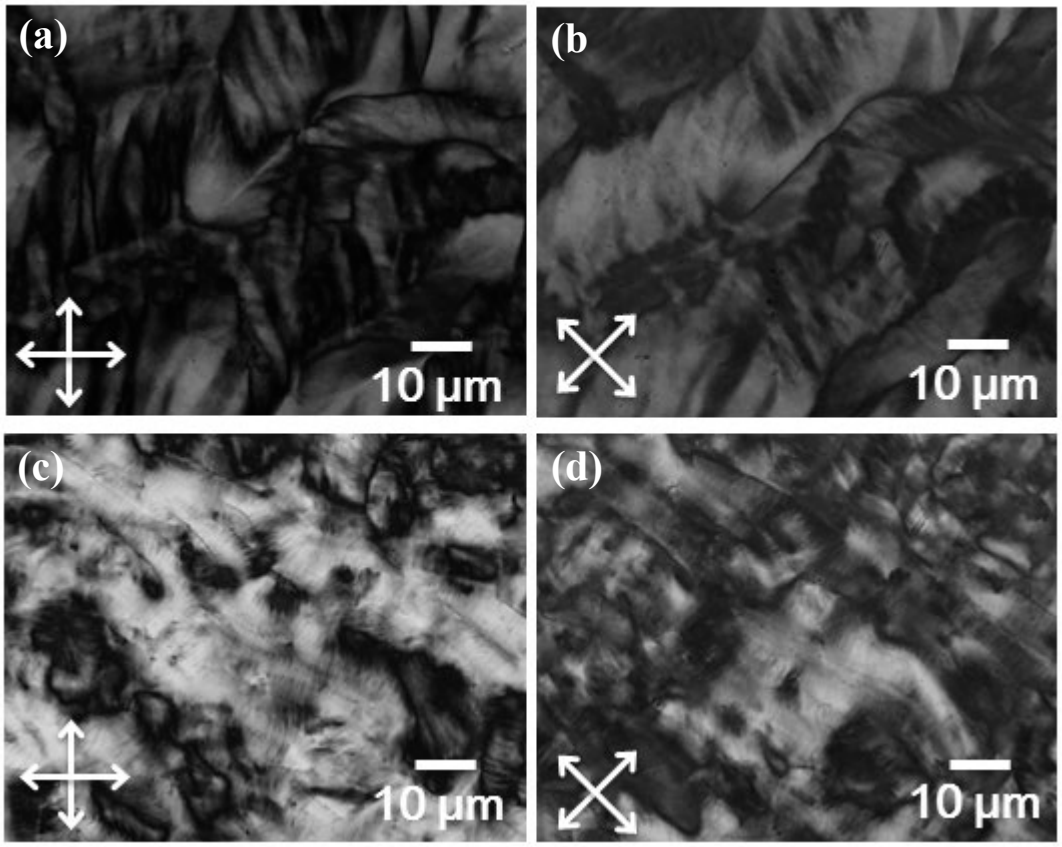

Fig. 1 Polarized optical micrograph (POM) images of the 400 nm SPI films at 0º and 45º. (a), (b) SPI thin film prepared without THF. (c), (d) SPI thin film prepared with THF.

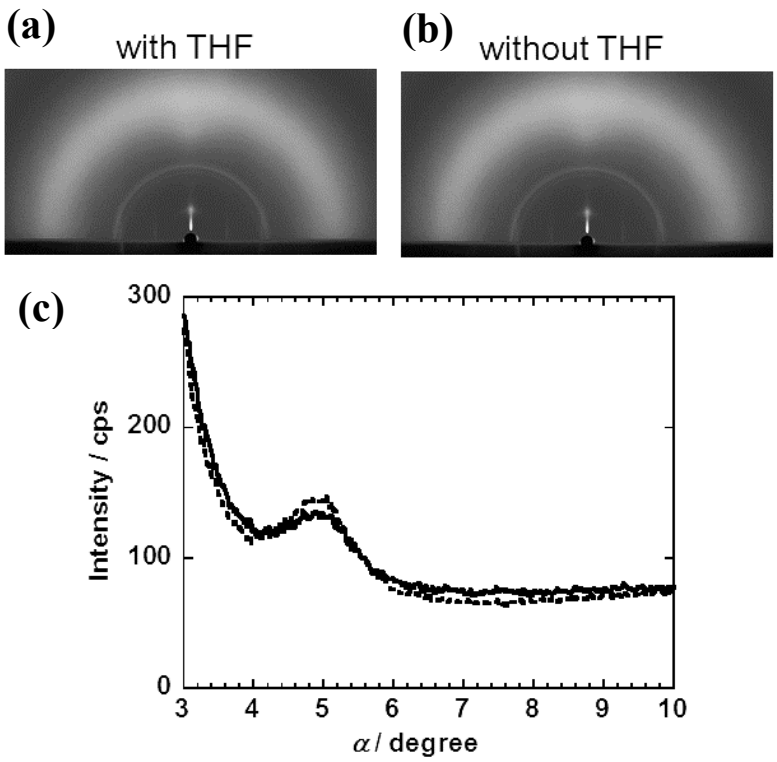

Fig. 2　GISAXS profiles of the two SPI thin films at RH = 40%. (a) 2D GISAXS profile of the SPI thin film prepared with THF. (b) 2D GISAXS profile of the SPI thin film prepared without THF. (c) 1D GISAXS profiles in the out-of-plane direction of the two SPI thin films prepared with THF and without THF. Dotted line and solid line are SPI thin films prepared with THF and without THF, respectively.

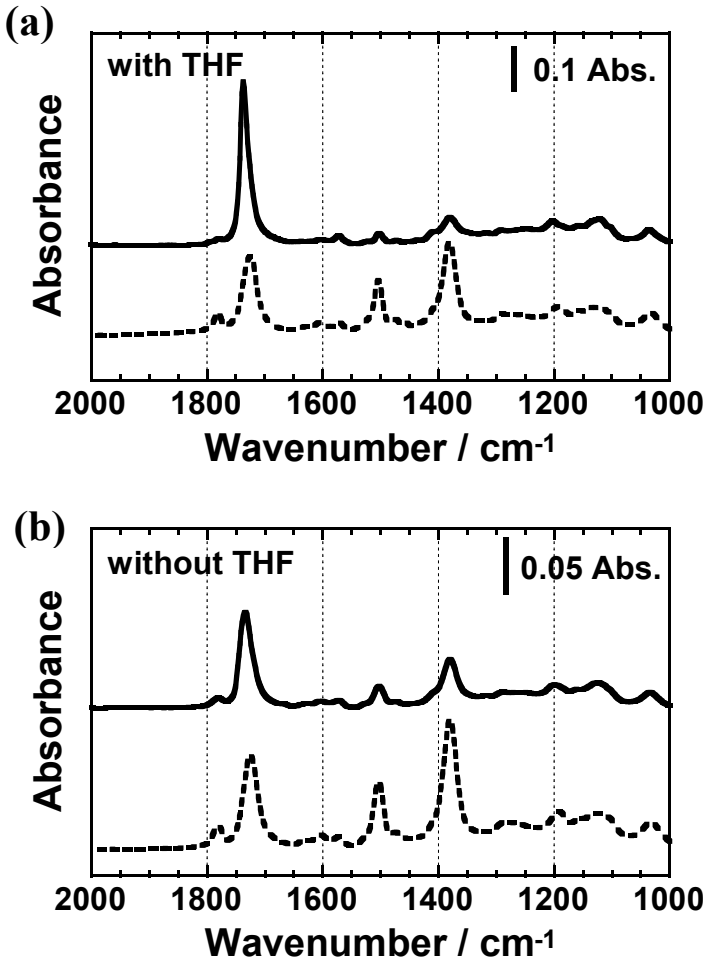

Fig. 3　pMAIR spectra for the two SPI thin films. (a) SPI thin film prepared without THF. (b) SPI thin film prepared with THF. Solid line and dotted line are OP and 2×IP spectra, respectively.

Graphical Index